Signal Processing 155 (2019) 182–192

Contents lists available at ScienceDirect

Signal Processing

journal homepage: www.elsevier.com/locate/sigpro

A nonlinear second-order filtering strategy for state estimation of uncertain systems

Hamed H. Afshari[a], S. Andrew Gadsden[b,*], Saeid Habibi[a]

[a] Centre for Mechatronics & Hybrid Technology, McMaster University, Hamilton, ON L8S 4L7, Canada
[b] Intelligent Control and Estimation Laboratory, University of Guelph, Guelph, ON N1G 2W1, Canada

ARTICLE INFO

Article history:
Received 8 October 2017
Revised 9 September 2018
Accepted 27 September 2018
Available online 28 September 2018

Keywords:
Nonlinear state estimation
Second-order filters
Electrohydrostatic actuator
Unmodeled uncertainties
External disturbances

ABSTRACT

In this paper, a new strategy referred to as the nonlinear second-order (NSO) filter is presented and used for estimation of linear and nonlinear systems in the presence of uncertainties. Similar to the popular Kalman filter estimation strategy, the proposed strategy is model-based and formulated as a predictor-corrector. The NSO filter is based on variable structure theory that utilizes a switching term and gain that ensures some level of estimation stability. It offers improvements in terms of robustness to modeling uncertainties and errors. The proof of stability is derived based on Lyapunov that demonstrates convergence of estimates towards the true state values. The proposed filtering strategy is based on a second-order Markov process that utilizes information from the current and past two time steps. An experimental system was setup and characterized in order to demonstrate the proposed filtering strategy's performance. The strategy was compared with the popular Kalman filter (and its nonlinear form) and the smooth variable structure filter (SVSF). Experimental results demonstrate that the proposed nonlinear second-order filter provides improvements in terms of state estimation accuracy and robustness to modeling uncertainties and external disturbances.

1. Introduction

Estimation is the process of extracting true state and parameter values from systems in the presence of noisy measurements, modeling uncertainties, and unwanted disturbances. This task aims to provide optimal estimates in terms of minimal estimation error, which is defined as the difference between the estimated and actual state values. Inherent to the estimation process is system and measurement noise, external disturbances, and uncertainties–all of which can be caused by sensors, instruments, or the environment. In order to overcome these issues, model-based estimation and filtering strategies are utilized to monitor and control engineering systems. In model-based methods, a probability density function (PDF) is calculated recursively, and is based on the state estimates. Information on the state mean and state covariance is contained within the PDF, and can be used to provide state estimates. Model-based strategies are recursive, and consist of two stages: predict and update. In the first stage, the system model is used to estimate (or predict) the state values at the next time step. The update stage, as the name suggests, refines the predicted state estimates based on system measurements. The most popular model-based method used for linear estimation problems is the well-known Kalman filter (KF) [1]. The KF assumes that the estimation problem is linear, the system is known, and the noise is zero-mean and Gaussian distributed. For general nonlinear and non-Gaussian systems, several strategies have been proposed: linearization (e.g., the extended Kalman filter or EKF [2,3]), and PDF approximation (e.g., the unscented Kalman filter or UKF [3], the cubature Kalman filter or CKF [4]). It has been demonstrated that the CKF is merely a special case of the UKF [4]. Due to improvements in computing power and reductions in cost, particle filters (PFs) have grown in popularity [5]. Similar to the UKF, the PF uses a large set of weighted particles that approximate the state PDF [3,6].

One of the main issues with the KF is that the estimation performance may degrade in the presence of modeling and parameter uncertainties. To overcome this issue, robust state estimation techniques are implemented, such as minimax estimators, worst-case, or set-membership state estimators [7,8]. From a statistical standpoint, the minimax estimators deal with uncertainties that are uniformly distributed within given bounds. In the case of ellipsoidal bounding sets, these estimators coincide with the KF for linear systems. Interestingly, there also exists minimax estimators where the uncertainty is mathematically expressed using entropy-like indexes [9]. Based on propagation of uncertainties, a family of

* Corresponding author.
E-mail address: gadsden@uoguelph.ca (S.A. Gadsden).

https://doi.org/10.1016/j.sigpro.2018.09.036

Nomenclature

$\mathbf{A}$	Linear state matrix
$\mathbf{A_E}$	Piston area
$\mathbf{B}$	Linear control matrix
$\mathbf{B_E}$	Load friction
$\mathbf{D_P}$	Pump displacement
$\mathbf{H}$	Linear measurement matrix
$\mathbf{K}$	Filter's gain
$\mathbf{L}$	Leakage coefficient
$\mathbf{M}$	Load mass
$\mathbf{P}$	State error covariance matrix
$\mathbf{Q}$	Process noise covariance matrix
$\mathbf{Q_e}$	Leakage flow rate
$\mathbf{Q_{L0}}$	Flow rate offset
$\mathbf{R}$	Measurement noise covariance matrix
$\mathbf{S}$	Vector of sliding variables
$\mathbf{T}$	Sampling rate
$\mathbf{V_0}$	Initial cylinder volume
$\mathbf{a_1,a_2,a_3}$	Friction coefficients
$\mathbf{e}$	Estimation error
$\mathbf{f}$	Nonlinear state model
$\mathbf{k}$	Sample time
$\mathbf{s}$	Sliding mode variable
$\mathbf{u}$	Control variable
$\mathbf{v}$	Measurement noise
$\mathbf{w}$	Process noise
$\mathbf{x}$	State vector
$\mathbf{z}$	Measurement vector
$\boldsymbol{\beta_e}$	Effective bulk modulus
$\boldsymbol{\gamma}$	Convergence rate
ε	Upper bound
$\boldsymbol{\omega_P}$	Motor rotational velocity
ψ	Smoothing boundary layer
$\hat{\square}$	Estimated quantity
$\square^{+}$	Pseudo-inverse operator

robust Kalman filter may be derived [10]. Other robust strategies include the so-called robust KF [11,12] and the H∞ filter [13]. The robust KF was used for systems with bounded modeling uncertainties such that an upper bound of the mean square estimation error (MSE) is minimized at each step [11]. Considerable research has been performed on the design of robust state estimation methods for dynamic systems with bounded uncertainties, such as mini-max estimators [14], worst-case [7,15], or set-membership state estimators [8]. Zames [13] created the H∞ method by removing the necessity of a perfect model or complete knowledge of the input statistics. The H∞ theory was designed by tracking the magnitude of the 'energy' of a signal for the worst possible scenario in terms of noise levels and modeling uncertainties.

In 2007, an initial form of the smooth variable structure filter (SVSF) was introduced based on variable structure theory introduced in the 1970s [16,17]. Similar to the KF method, the SVSF [17] is a predictor-corrector strategy. However, the SVSF formulation is unique since the gain is derived based on a discontinuous corrective gain. This gain bounds state estimates to within a region of the true state trajectory, improving stability of estimates and robustness to external disturbances [17]. The discontinuous corrective action provided by the SVSF gain has demonstrated robustness to bounded modeling uncertainties [18,19]. A smoothing term (e.g., saturation function) is used to suppress or smooth chatter caused by the SVSF gain [20]. However, the robustness of the method comes at a trade-off; the SVSF introduced in 2007 is a sub-optimal filter [21,22]. Gadsden extended the SVSF by deriving a state error covariance term for it, and using the term to obtain an optimal smoothing boundary layer [18,19]. Results demonstrate improved state estimation while maintaining robustness to modeling uncertainties and disturbances [18,19,23]. Afshari et al. have researched on the design and application of hydraulic and pneumatic actuation systems. They implemented a number of techniques to analyze the dynamic behavior of such systems [24,25]. Moreover, Afshari et al. investigated the performance of popular robust estimation methods with applications to fault detection and diagnosis [26–29], maneuver vehicle tracking [30–32], and energy management systems [33,34].

This paper is motivated by state estimation problems for systems with modeling uncertainties or errors, such as in fault operating conditions. Since a higher-order version of the SVSF is derived, it is expected that the proposed method will yield a more accurate solution to the estimation problem in terms of state error. However, the higher-order accuracy comes at a trade-off with computational complexity and time. Since computers are being extremely fast and relatively cheap, the issue of computational power requirements is less important than a decade ago. During system faults, the mathematical model of the system used by the filter deviates from the true model (e.g., normal conditions). In most cases it is extremely difficult (or impossible) to identify all of the possible operating and fault conditions. The proposed NSO filter, described in Section 2, is able to overcome this issue by generating state estimates for systems subjected to 'soft' fault conditions. The stability of the proposed filter is proven mathematically. Different measurement cases (full and reduced) for the proposed filter are described in Sections 3 and 4, respectively. An experimental setup was used to verify and compare the proposed NSO filter with the popular KF and the EKF. As described in Section 5, two cases were studied: linear system with only one measured state, and nonlinear system with full measurements. The paper is concluded in Section 6.

2. NSO filtering strategy

The proposed NSO filter is based on the SVSF, whereby a second-order formulation of the gain is implemented [17]. The strategy can be formulated to work with linear and nonlinear systems. However, for nonlinear systems without full measurements, the nonlinearities need to be linearized or approximated. A technique is presented in [17] to obtain the gain for unmeasurable states of a nonlinear system without the need for linearization. The proposed filter utilizes a prediction and update stage (described in this section). To formulate the NSO filter, consider a nonlinear system represented by a discrete state model as follows:

$$\mathbf{x}_{k+1} = \mathbf{F}(\mathbf{x}_k, \mathbf{u}_k, \mathbf{w}_k), \tag{1}$$

where $\mathbf{F} : \mathbb{R}^{2n+p} \to \mathbb{R}^n$ is the nonlinear state model, $\mathbf{x}_k \in \mathbb{R}^{n\times 1}$ is the state vector, $\mathbf{u}_k \in \mathbb{R}^{p\times 1}$ is the control vector, and $\mathbf{w}_k \in \mathbb{R}^{n\times 1}$ is the process noise (modeling uncertainties) vector. The measurement model is assumed to be linear or at least piece-wise linear such that:

$$\mathbf{z}_k = \mathbf{H}\mathbf{x}_k + \mathbf{v}_k, \tag{2}$$

where $\mathbf{z}_k \in \mathbb{R}^{m\times 1}$ is the measurement vector, $\mathbf{v}_k \in \mathbb{R}^{m\times 1}$ is the measurement noise, and $\mathbf{H} \in \mathbb{R}^{m\times n}$ is the measurement matrix.

Assumption 1: The control vector $\mathbf{u}_k$ is assumed known and norm-bounded. Moreover, vectors $\mathbf{w}_k$ and $\mathbf{v}_k$ are assumed to be unknown but norm-bounded, and with a zero mean.

Assumption 2: It is assumed that the system with Eqs. (1) and (2) is smooth and with continuous partial derivatives.

Based on these assumptions, consider the following steps for the NSO filter.

Prediction stage:

(1) The *a priori* state estimate vector is predicted as follows:

$$\hat{\mathbf{x}}_{k+1|k} = \mathbf{F}(\hat{\mathbf{x}}_{k|k}, \mathbf{u}_k), \tag{3}$$

The *a priori* state estimate $\hat{\mathbf{x}}_{k+1|k}$ is produced using the state model $\mathbf{F}$ and the previous *a posteriori* state estimate $\hat{\mathbf{x}}_{k|k}$. An initial estimate $\hat{\mathbf{x}}_0 \in \mathbb{R}^{n\times 1}$ is required to initialize or start the process. The *a priori* measurement vector estimate $\hat{\mathbf{z}}_{k+1|k}$ is also given by:

$$\hat{\mathbf{z}}_{k+1|k} = \mathbf{H}\hat{\mathbf{x}}_{k+1|k}. \tag{4}$$

(2) The *a posteriori* measurement error $\mathbf{e}_{\mathbf{z_{k|k}}} \in \mathbb{R}^{m\times 1}$ and *a priori* measurement error vector $\mathbf{e}_{\mathbf{z_{k+1|k}}} \in \mathbb{R}^{m\times 1}$ are respectively given by:

$$\mathbf{e}_{\mathbf{z_{k|k}}} = \mathbf{z}_k - \mathbf{H}\hat{\mathbf{x}}_{k|k}, \tag{5}$$

$$\mathbf{e}_{\mathbf{z_{k+1|k}}} = \mathbf{z}_{k+1} - \mathbf{H}\hat{\mathbf{x}}_{k+1|k}. \tag{6}$$

Update stage:

(3) A corrective gain for the NSO filter, $\mathbf{K}_{k+1} \in \mathbb{R}^{n\times m}$, is obtained as a nonlinear function of the *a priori* measurement error $\mathbf{e}_{\mathbf{z_{k+1|k}}}$and the *a posteriori* errors $\mathbf{e}_{\mathbf{z_{k|k}}}and\mathbf{e}_{\mathbf{z_{k-1|k-1}}}$as:

$$\mathbf{K}_{k+1} = \mathbf{f}(\mathbf{H}, \mathbf{e}_{\mathbf{z_{k+1|k}}}, \mathbf{e}_{\mathbf{z_{k|k}}}, \mathbf{e}_{\mathbf{z_{k-1|k-1}}}). \tag{7}$$

In this paper, $\mathbf{H}$ is initially assumed to be full rank indicating that all states are measured, $m = n$. The corrective gain of the nonlinear 2nd-order filter for cases with full state measurement $(m = n)$ and cases without full state measurement $(m < n)$ is described in Sections 3 and 4, respectively.

(4) The *a priori* estimates are utilized to obtain *a posteriori* estimates $\hat{\mathbf{x}}_{k+1|k+1}$ such that:

$$\hat{\mathbf{x}}_{k+1|k+1} = \hat{\mathbf{x}}_{k+1|k} + \mathbf{K}_{k+1}. \tag{8}$$

(5) Steps 1–4 are iteratively repeated for each sample time.

Assumption 3: In order to apply the NSO filter, it is assumed that both the state and measurement models can be mapped to each other [17]. Without noise and uncertainties, it is possible to find an inverse mapping that generates $\mathbf{x}_k$ by iterations of the output vector in the form of $\mathbf{x}_{n_k} = \mathbf{F}_n^{-1}(\mathbf{H}^{+}\mathbf{z}_{k+1}, \mathbf{H}^{+}\mathbf{z}_k, \mathbf{u}_k)$ [17]. Note that $\mathbf{H}^{+}$ denotes pseudo-inverse of the $\mathbf{H}$ matrix, where $m \neq n$.

The SVSF presented in [17] was based on the a prior measurement and a posteriori measurement errors. However, NSO includes an additional a posteriori measurement error, as described by Eq. (7). As demonstrated later, this improves the estimation accuracy at a cost of slightly increased computational complexity.

3. The NSO filtering strategy for fully measured systems ($m = n$)

To ensure robustness, the corrective gain $\mathbf{K}_{k+1}$ for the NSO filtering strategy must satisfy the Lyapunov's second law for stability. *Theorem 1* presents a stable corrective gain restricted to systems with a full measurement matrix $\mathbf{H} \in \mathbb{R}^{m\times n}(m = n)$. Thereafter, Section 4 presents the gain for cases with fewer measurements than states $(m < n)$.

Definition 1. Let Δ be the backward difference operator that applies to variable x such that: $\Delta\mathbf{x}_{k+1} = \mathbf{x}_{k+1} - \mathbf{x}_k$. It is assumed that Δ is smooth and differentiable.

Theorem 1. *The NSO filter with the corrective gain (9) is considered stable, and will generate state estimates that converge to the true state trajectory:*

$$\mathbf{K}_{k+1} = \mathbf{H}^{-1}\left[\mathbf{e}_{z_{k+1|k}} - \frac{\mathbf{e}_{z_{k|k}}}{2} - \gamma\sqrt{\frac{\mathbf{e}_{z_{k|k}}\circ\mathbf{e}_{z_{k|k}}}{4} + \frac{\Delta\mathbf{e}_{z_{k|k}}\circ\Delta\mathbf{e}_{z_{k|k}}}{2}}\right], \tag{9}$$

where $\mathbf{H} \in \mathbb{R}^{m\times n}(m = n)$ is the measurement matrix, $\mathbf{e}_{z_{k|k}} \in \mathbb{R}^{m\times 1}$ is the measurement error vector, $\Delta\mathbf{e}_{z_{k|k}} = \mathbf{e}_{z_{k|k}} - \mathbf{e}_{z_{k-1|k-1}}$ is the time difference of the measurement error vector, and γ is a constant coefficient and is defined such that $0 < \gamma < 1$. Note that $\circ$ denotes the Schur (element-wise) product, and the square root operator applies to $\mathbf{e}_{z_{k|k}}$ and $\Delta\mathbf{e}_{z_{k|k}}$ element-wisely.

Proof: Consider a Lyapunov function candidate that utilizes the measurement error vector and its discrete-time form, as follows:

$$\mathbf{V}_k = \mathbf{e}_{z_{k|k}} \circ \mathbf{e}_{z_{k|k}} + \Delta\mathbf{e}_{z_{k|k}} \circ \Delta\mathbf{e}_{z_{k|k}}, \tag{10}$$

where Δ refers to the backward difference, and where$\circ$ denotes the Schur product. Based on Lyapunov's theory, the system is stable if: $\Delta\mathbf{V}_{k+1} = \mathbf{V}_{k+1} - \mathbf{V}_k < 0$. Multiplying both sides of the gain in (9) by $\mathbf{H}$ and rearranging yield the following:

$$\mathbf{e}_{z_{k+1|k}} - \mathbf{H}\mathbf{K}_{k+1} = \frac{\mathbf{e}_{z_{k|k}}}{2} + \gamma\sqrt{\frac{\mathbf{e}_{z_{k|k}}\circ\mathbf{e}_{z_{k|k}}}{4} + \frac{\Delta\mathbf{e}_{z_{k|k}}\circ\Delta\mathbf{e}_{z_{k|k}}}{2}}. \tag{11}$$

Following Eq. (8), the corrective gain may be restated as: $\mathbf{K}_{k+1} = \hat{\mathbf{x}}_{k+1|k+1} - \hat{\mathbf{x}}_{k+1|k}$. Substituting this relation into (11) yields:

$$\mathbf{e}_{z_{k+1|k}} - \mathbf{H}(\hat{\mathbf{x}}_{k+1|k+1} - \hat{\mathbf{x}}_{k+1|k}) = \frac{\mathbf{e}_{z_{k|k}}}{2} + \gamma\sqrt{\frac{\mathbf{e}_{z_{k|k}}\circ\mathbf{e}_{z_{k|k}}}{4} + \frac{\Delta\mathbf{e}_{z_{k|k}}\circ\Delta\mathbf{e}_{z_{k|k}}}{2}}. \tag{12}$$

The predicted and updated measurement errors at time k are given by Eqs. (5) and (6) as: $\mathbf{e}_{z_{k+1|k}} = \mathbf{z}_{k+1} - \mathbf{H}\hat{\mathbf{x}}_{k+1|k}$ and $\mathbf{e}_{z_{k+1|k+1}} = \mathbf{z}_{k+1} - \mathbf{H}\hat{\mathbf{x}}_{k+1|k+1}$. Subtracting the predicted error from the updated error yields the following:

$$\mathbf{e}_{z_{k+1|k+1}} - \mathbf{e}_{z_{k+1|k}} = -\mathbf{H}(\hat{\mathbf{x}}_{k+1|k+1} - \hat{\mathbf{x}}_{k+1|k}). \tag{13}$$

Using Eq. (13), equality (12) may be restated as follows:

$$\mathbf{e}_{z_{k+1|k+1}} = \frac{\mathbf{e}_{z_{k|k}}}{2} + \gamma\sqrt{\frac{\mathbf{e}_{z_{k|k}}\circ\mathbf{e}_{z_{k|k}}}{4} + \frac{\Delta\mathbf{e}_{z_{k|k}}\circ\Delta\mathbf{e}_{z_{k|k}}}{2}}. \tag{14}$$

Transferring $\mathbf{e}_{z_{k|k}}/2$ in equality (14) to the left side of the equation, and squaring both sides of the equation using the Schur product, it becomes:

$$\left(\mathbf{e}_{z_{k+1|k+1}} - \frac{\mathbf{e}_{z_{k|k}}}{2}\right) \circ \left(\mathbf{e}_{z_{k+1|k+1}} - \frac{\mathbf{e}_{z_{k|k}}}{2}\right) = \gamma^2\left(\frac{\mathbf{e}_{z_{k|k}}\circ\mathbf{e}_{z_{k|k}}}{4} + \frac{\Delta\mathbf{e}_{z_{k|k}}\circ\Delta\mathbf{e}_{z_{k|k}}}{2}\right). \tag{15}$$

Since γ is defined such that $0 < \gamma < 1$, equality (15) is restated as:

$$\left(\mathbf{e}_{z_{k+1|k+1}} - \frac{\mathbf{e}_{z_{k|k}}}{2}\right) \circ \left(\mathbf{e}_{z_{k+1|k+1}} - \frac{\mathbf{e}_{z_{k|k}}}{2}\right) < \left(\frac{\mathbf{e}_{z_{k|k}}\circ\mathbf{e}_{z_{k|k}}}{4} + \frac{\Delta\mathbf{e}_{z_{k|k}}\circ\Delta\mathbf{e}_{z_{k|k}}}{2}\right). \tag{16}$$

Expanding the above inequality leads to:

$$\mathbf{e}_{z_{k+1|k+1}} \circ \mathbf{e}_{z_{k+1|k+1}} - \mathbf{e}_{z_{k+1|k+1}} \circ \mathbf{e}_{z_{k|k}} < (\Delta\mathbf{e}_{z_{k|k}} \circ \Delta\mathbf{e}_{z_{k|k}})/2. \tag{17}$$

Adding and subtracting $(\mathbf{e}_{z_{k|k}} \circ \mathbf{e}_{z_{k|k}})/2$ into the left hand side of the above and rearranging yields the following:

$$2\mathbf{e}_{z_{k+1|k+1}} \circ \mathbf{e}_{z_{k+1|k+1}} - 2\mathbf{e}_{z_{k+1|k+1}} \circ \mathbf{e}_{z_{k|k}} + \mathbf{e}_{z_{k|k}} \circ \mathbf{e}_{z_{k|k}} - \mathbf{e}_{z_{k|k}} \circ \mathbf{e}_{z_{k|k}} - \Delta\mathbf{e}_{z_{k|k}} \circ \Delta\mathbf{e}_{z_{k|k}} < 0. \tag{18}$$

Equality (18) may be restated such that:

$$\mathbf{e}_{z_{k+1|k+1}} \circ \mathbf{e}_{z_{k+1|k+1}} + (\mathbf{e}_{z_{k+1|k+1}} - \mathbf{e}_{z_{k|k}}) \circ (\mathbf{e}_{z_{k+1|k+1}} - \mathbf{e}_{z_{k|k}}) - \mathbf{e}_{z_{k|k}} \circ \mathbf{e}_{z_{k|k}} - \Delta\mathbf{e}_{z_{k|k}} \circ \Delta\mathbf{e}_{z_{k|k}} < 0. \tag{19}$$

According to the Lyapunov function, given by $\mathbf{V}_k = \mathbf{e}_{z_{k|k}} \circ \mathbf{e}_{z_{k|k}} + \Delta\mathbf{e}_{z_{k|k}} \circ \Delta\mathbf{e}_{z_{k|k}}$, inequality (19) becomes:

$$\Delta\mathbf{V}_{k+1} < 0. \tag{20}$$

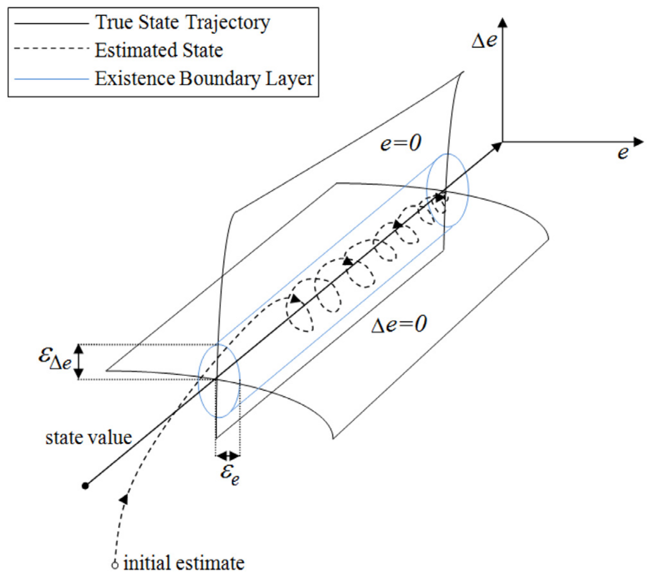

Fig. 1. Illustrative concept of the NSO filter.

Remark 1. An intuitive result of *Theorem 1* is that if the stability criterion (10) is preserved, then absolute values of the measurement error will decrease over time. However, factors such as the measurement noise, modeling and parametric uncertainties, discretization error and measurement errors cannot be canceled completely. Since the measurement and the process noise are assumed to be norm-bounded with zero mean, it is deduced that they only decrease until reaching a subspace bounded by ε_e and $\varepsilon_{\Delta e}$, respectively. Thereafter, the measurement error remains bounded such that $||\mathbf{e}_{z_{k|k}}|| < \varepsilon_e$ and $||\boldsymbol{\Delta}\mathbf{e}_{z_{k|k}}|| < \varepsilon_{\Delta e}$.

Remark 2. Following equality (15), γ may be referred to as the convergence rate coefficient, since proper selection of γ such that $0 < \gamma < 1$ preserves the stability and convergence of the filter.

Remark 3. The NSO filter can be applied to nonlinear systems with full measurements ($m = n$), without the need for linearization or approximation. This capability is an advantage of this method over other estimation methods that are using linearization (e.g., EKF [2]) or some form of approximation of nonlinear terms (e.g., UKF [3] or CKF [4]). However, the NSO filter does require a linear or piecewise linear measurement model. Note that, however, for cases without full state measurement ($m < n$), the nonlinear state model needs to be linearized.

Fig. 1 shows the main concept of the NSO filter. As shown in the figure, an initial state estimate is made utilizing the state model (known or estimated). The NSO corrective gain pushes the estimated state trajectory in a path that leads it within a region of the actual state trajectory. This region is referred to as the boundary layer. The width of this layer depends on the amount of modeling and parameter uncertainties, measurement noise, and other factors such as sample time, discretization error, and so forth. The width is typically defined by design, and can be tuned. Once within the existence subspace, the stability criterion guarantees that the estimated state remains in a close vicinity of the actual state, assuming norm-bounded noise and uncertainties. In this context, the measurement error $\mathbf{e}_{z_{k|k}}$ and its time difference $\boldsymbol{\Delta}\mathbf{e}_{z_{k|k}}$ may be bounded by two upper bounds such as ε_e and $\varepsilon_{\Delta e}$, respectively.

In the NSO filter, the stability criterion applies constraints on both the measurement error $\mathbf{e}_{z_{k|k}}$ and its time difference $\boldsymbol{\Delta}\mathbf{e}_{z_{k|k}}$. Whereas, in the other first-order filters (e.g., KF and SVSF), there exists only one constraint that applies to only the measurement error $\mathbf{e}_{z_{k|k}}$. This characteristic will increase the accuracy of the NSO filter with respect to first-order filters for state estimation under uncertain conditions (as per Fig. 2). Moreover, the corrective gain (9) value at $k+1$ computationally depends on the values of the measurement error at k and $k-1$, namely $\mathbf{e}_{z_{k|k}}$ and $\mathbf{e}_{z_{k-1|k-1}}$. This means that the filter updates the *a priori* state estimates at $k+1$ based on information available from two time steps before. Hence, it utilizes more information from the past which results in a smooth estimate (i.e., smoothing filter), and consequently reduces undesirable effects of noise, spikes, and other high frequency dynamics on state estimates.

4. NSO filter for linear systems with $m < n$

The NSO filter may be applied to linear systems with more states than measurements ($m < n$), if the system is both controllable and observable. In this case, the corrective gain of the filter is calculated based on the Luenberger's observer, as presented in [17]. In this context, the system nonlinearities (1) must be linearized as per the following:

$$\mathbf{x}_{k+1} = \mathbf{A}\mathbf{x}_k + \mathbf{B}\mathbf{u}_k + \mathbf{w}_k, \tag{21}$$

where $\mathbf{A} \in \mathbb{R}^{n\times n}$ is the state matrix, $\mathbf{B} \in \mathbb{R}^{p\times 1}$ is the control matrix. The state variables may be decomposed into two parts $\mathbf{x} = [\ \mathbf{x}_u \quad \mathbf{x}_l\ ]^T$, where the upper part $\mathbf{x}_u \in \mathbb{R}^{m\times 1}$ is directly measured and whereas the lower part $\mathbf{x}_l \in \mathbb{R}^{(n-m)\times 1}$ is not. Using the Luenberger's transformation, a new measurement vector is given by [17]:

$$\mathbf{T}\mathbf{x}_k = \begin{bmatrix} \mathbf{y}_{u_k} & \mathbf{y}_{l_k} \end{bmatrix}^T, \tag{22}$$

where $\mathbf{T}$ is defined as a transformation matrix. Thereafter, a modified state vector may be provided in terms of measurements as: $\mathbf{y} = [\mathbf{z} \quad \mathbf{y}_l]^T$, where $\mathbf{z} \in \mathbb{R}^{m\times 1}$ is the measurements and $\mathbf{y}_l \in \mathbb{R}^{(n-m)\times 1}$ are the 'artificial' measurements. Values for entries of $\mathbf{y}_l$ are obtained using the partitioned model. The measurement model is given by [17]:

$$\begin{bmatrix} \mathbf{z}_{k+1} \\ \mathbf{y}_{l_{k+1}} \end{bmatrix} = \begin{bmatrix} \boldsymbol{\Phi}_{11} & \boldsymbol{\Phi}_{12} \\ \boldsymbol{\Phi}_{21} & \boldsymbol{\Phi}_{22} \end{bmatrix} \begin{bmatrix} \mathbf{z}_k \\ \mathbf{y}_{l_k} \end{bmatrix} + \begin{bmatrix} \mathbf{G}_1 \\ \mathbf{G}_2 \end{bmatrix} \mathbf{u}_k + \begin{bmatrix} \mathbf{d}_1 \\ \mathbf{d}_2 \end{bmatrix} \mathbf{w}_k, \tag{23}$$

where $\boldsymbol{\Phi} = \mathbf{T}^{-1}\mathbf{A}\mathbf{T}$, $\mathbf{G} = \mathbf{T}^{-1}\mathbf{B}$, and $\mathbf{d} = \mathbf{T}^{-1}$. The *a priori* state estimate is calculated by [17]:

$$\begin{bmatrix} \hat{\mathbf{z}}_{k+1|k} \\ \hat{\mathbf{y}}_{l_{k+1|k}} \end{bmatrix} = \begin{bmatrix} \boldsymbol{\Phi}_{11} & \boldsymbol{\Phi}_{12} \\ \boldsymbol{\Phi}_{21} & \boldsymbol{\Phi}_{22} \end{bmatrix} \begin{bmatrix} \mathbf{z}_k \\ \hat{\mathbf{y}}_{l_{k|k}} \end{bmatrix} + \begin{bmatrix} \mathbf{G}_1 \\ \mathbf{G}_2 \end{bmatrix} \mathbf{u}_k. \tag{24}$$

Subtracting (24) from (23), the predicted and updated measurement errors for the hidden measurement vector $\mathbf{y}_l$ are determined respectively as follows [17]:

$$\mathbf{e}_{y_{l,k|k}} = \boldsymbol{\Phi}_{12}{}^{-1}\mathbf{e}_{z_{k+1|k}}, \tag{25}$$

$$\mathbf{e}_{y_{l,k+1|k}} = \boldsymbol{\Phi}_{22}\boldsymbol{\Phi}_{12}{}^{-1}\mathbf{e}_{z_{k+1|k}}, \tag{26}$$

where $\mathbf{e}_{y_l} \in \mathbb{R}^{(n-m)\times 1}$ is the artificial measurement error vector and $\mathbf{e}_z \in \mathbb{R}^{m\times 1}$ is the measurement error vector corresponding to measurable states. Eqs. (25) and (26) present a mapping of the measurement error vector. They are used for obtaining a corrective gain for the lower partition of states as follows:

$$\mathbf{K}_{k+1} = \boldsymbol{\Phi}_{22}\boldsymbol{\Phi}_{12}^{-1} e_{z_{k+1|k}} - \frac{\boldsymbol{\Phi}_{12}^{-1}\mathbf{e}_{z_{k|k}}}{2} - \gamma\,\boldsymbol{\Phi}_{12}^{-1}\sqrt{\frac{\mathbf{e}_{z_{k|k}}\circ\mathbf{e}_{z_{k|k}}}{4} + \frac{\Delta\mathbf{e}_{z_{k|k}}\circ\Delta\mathbf{e}_{z_{k|k}}}{2}}. \tag{27}$$

Considering the elements within the state vector, the corrective gain for the NSO filter is formulated for linear systems with more

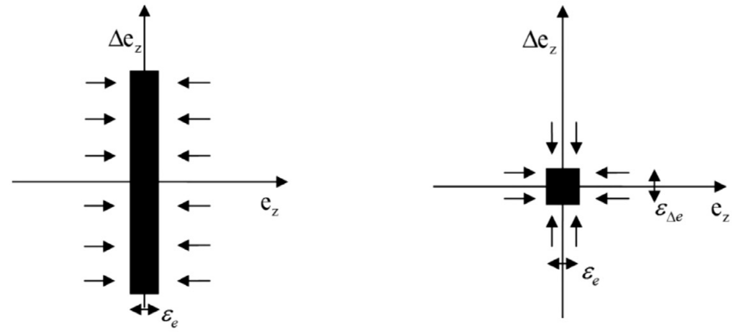

a) Error by a 1st-order filter = $O(\varepsilon_s)$ **b)** Error by a 2nd-order filter = $O(\varepsilon_s, \varepsilon_{\Delta s})$

Fig. 2. Comparison of error by a 2nd-order filter and by a 1st-order filter.

states than measurements as follows:

$$\mathbf{K}_{k+1} = \begin{cases} \mathbf{H}^{+}\left(\mathbf{e}_{z_{k+1|k}} - \frac{\mathbf{e}_{z_{k|k}}}{2} - \gamma\sqrt{\frac{\mathbf{e}_{z_{k|k}}\circ\mathbf{e}_{z_{k|k}}}{4} + \frac{\Delta\mathbf{e}_{z_{k|k}}\circ\Delta\mathbf{e}_{z_{k|k}}}{2}}\right), \\ \mathbf{\Phi}_{22}\mathbf{\Phi}_{12}^{-1}e_{z_{k+1|k}} - \frac{\mathbf{\Phi}_{12}^{-1}\mathbf{e}_{z_{k|k}}}{2} - \gamma\,\mathbf{\Phi}_{12}^{-1}\sqrt{\frac{\mathbf{e}_{z_{k|k}}\circ\mathbf{e}_{z_{k|k}}}{4} + \frac{\Delta\mathbf{e}_{z_{k|k}}\circ\Delta\mathbf{e}_{z_{k|k}}}{2}} \end{cases}. \tag{28}$$

where $\mathbf{H}^{+}$ is the pseudo-inverse of $\mathbf{H} \in \mathbb{R}^{m\times n}$ that is not square. The upper part of (28) shows the corrective gain for measurable states, whereas the lower part shows the gain for hidden states.

Lemma 1. The NSO filter under the gain (27) produces stable state estimates for the lower partition states $\mathbf{y}_l$.

Proof. Let define a Lyapunov function candidate for the lower partition states $\mathbf{y}_l \in \mathbb{R}^{(n-m)\times 1}$ in terms of $\mathbf{e}_{y_l} \in \mathbb{R}^{(n-m)\times 1}$, as follows:

$$\mathbf{V}_k = \mathbf{e}_{y_{l,k|k}}{}^{\circ}\mathbf{e}_{y_{l,k|k}} + \Delta\mathbf{e}_{y_{l,k|k}}{}^{\circ}\Delta\mathbf{e}_{y_{l,k|k}}. \tag{29}$$

Since $\mathbf{e}_{y_{l,k|k}} = \mathbf{\Phi}_{12}{}^{-1}\mathbf{e}_{z_{k+1|k}}$, and $\mathbf{e}_{y_{l,k+1|k}} = \mathbf{\Phi}_{22}\mathbf{\Phi}_{12}{}^{-1}\mathbf{e}_{z_{k+1|k}}$, the corrective gain (27) for the lower partition states is restated as follows:

$$\mathbf{K}_{l_{k+1}} = \mathbf{e}_{y_{l,k+1|k}} - \frac{\mathbf{e}_{y_{l,k|k}}}{2} - \gamma\sqrt{\frac{\mathbf{e}_{y_{l,k|k}}{}^{\circ}\mathbf{e}_{y_{l,k|k}}}{4} + \frac{\Delta\mathbf{e}_{y_{l,k|k}}{}^{\circ}\Delta\mathbf{e}_{y_{l,k|k}}}{2}}. \tag{30}$$

The stability proof of Eqs. (11–20) may simply be repeated for the lower partition states using the gain (30). The time difference of the Lyapunov function (29) is hence given by:

$$\mathbf{e}_{y_{l,k+1|k+1}}{}^{\circ}\mathbf{e}_{y_{l,k+1|k+1}} + (\mathbf{e}_{y_{l,k+1|k+1}} - \mathbf{e}_{y_{l,k|k}})^{\circ}(\mathbf{e}_{y_{l,k+1|k+1}} - \mathbf{e}_{y_{l,k|k}}) - \mathbf{e}_{y_{l,k|k}} - \Delta\mathbf{e}_{y_{l,k|k}}{}^{\circ}\Delta\mathbf{e}_{y_{l,k|k}} < 0. \tag{31}$$

Since $\mathbf{V}_k = \mathbf{e}_{y_{l,k|k}}{}^{\circ}\mathbf{e}_{y_{l,k|k}} + \Delta\mathbf{e}_{y_{l,k|k}}{}^{\circ}\Delta\mathbf{e}_{y_{l,k|k}}$, inequality (31) is restated as $\Delta\mathbf{V}_{k+1} < 0$ that proves stability of the filter under gain (27). □

5. Application to an experimental electrohydrostatic actuator (EHA) setup

To illustrate the accuracy and efficacy of the proposed NSO filter, a flight-surface actuator system referred to the electrohydrostatic actuator (EHA) was used. The EHA is an experimental setup that has been devised and fabricated based on existing technology. The experimental setup and its circuit diagram are presented in Figs. 3 and 4, respectively. Additional EHA details are available in the Appendix.

The EHA dynamics can be defined by three kinematic statics: actuator position x_1, velocity x_2, and acceleration x_3 [19]. Gadsden developed a nonlinear system model of the EHA based on mathematical modeling and system identification, as per [19]:

$$x_{1,k+1} = x_{1,k} + Tx_{2,k}, \tag{32}$$

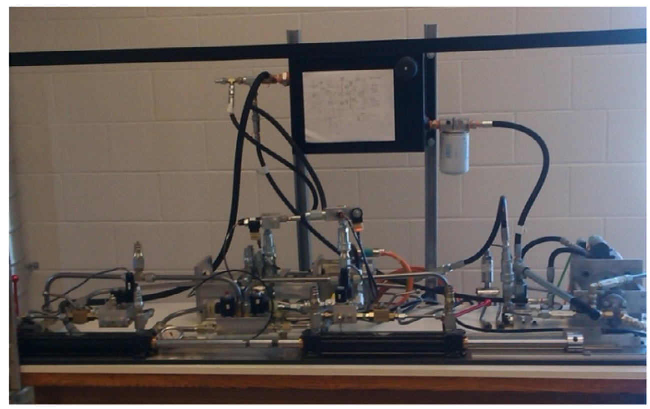

Fig. 3. Experimental setup of the electrohydrostatic actuator (EHA).

Table 1
The parameters used to define the EHA system [19].

Parameter	Physical meaning	Parameter values
A_E	Piston area	1.52×10^{-3} m^2
D_P	Pump displacement	5.57×10^{-7} m^3/rad
L	Leakage coefficient	4.78×10^{-12} m^3/(sec × Pa)
M	Load mass	7.376 Kg
Q_{L0}	Flow rate offset	2.41×10^{-6} m^3/sec
V_0	Initial cylinder volume	1.08×10^{-3} m^3
β_e	Effective bulk modulus	2.07×10^{8} Pa

$$x_{2,k+1} = x_{2,k} + Tx_{3,k}, \tag{33}$$

$$x_{3,k+1} = \left[1 - T\frac{a_2V_0 + M\beta_eL}{MV_0}\right]x_{3,k} - T\frac{\left(A_E{}^2 + a_2L\right)\beta_e}{MV_0}x_{2,k} - T\frac{2a_1V_0x_{2,k}x_{3,k} + \beta_eL\left(a_1x_{2,k}{}^2 + a_3\right)}{MV_0}\mathrm{sgn}(x_{2,k}) + T\frac{A_E\beta_e}{MV_0}u_k, \tag{34}$$

where V_0 is the initial cylinder volume, β_e is the stiffness of the hydraulic fluid or known as the effective bulk modulus, A_E is the cross-sectional area of the piston, L is the coefficient for leakage, and M is the mass of the load. Moreover, T represents the sample time and is equal to $T = 1$ ms. These parameters are described and listed in Table 1. The input to the EHA is defined such that it adjusts the fluid flow rate as follows [19]:

$$u = D_p\omega_p - \mathrm{sgn}(P_1 - P_2)Q_{L0}, \tag{35}$$

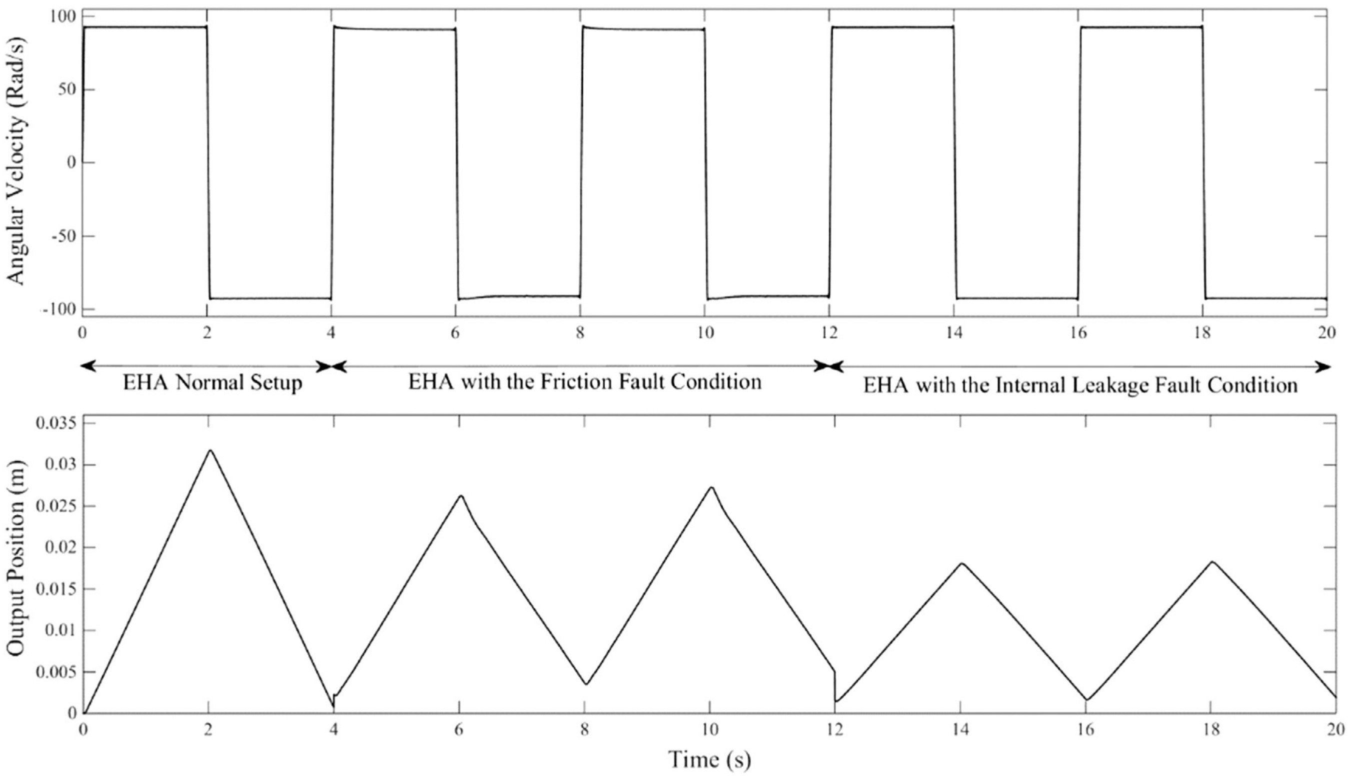

Fig. 4. EHA input and output signals under three operating conditions.

Table 2
Numeric values of the friction coefficients [19].

Condition	a_1	a_2	a_3
Normal	6.589×10^4	2.144×10^3	436
Major friction	1.162×10^6	-7.440×10^3	500
Minor friction	4.462×10^6	1.863×10^4	551

Table 3
Numeric values of leakage coefficients and flow rate offsets [19].

Condition	Leakage (L)	Flow rate (Q_{L0})
Normal	4.78×10^{-12} m^3/(sec × Pa)	2.41×10^{-6} m^3/s
Major leakage	2.52×10^{-11} m^3/(sec × Pa)	1.38×10^{-5} m^3/s
Minor leakage	6.01×10^{-11} m^3/(sec × Pa)	1.47×10^{-5} m^3/s

where D_p is the hydraulic displacement by the pump, Q_l is the flow rate of the leakage, and Q_{l0} is an adjustment parameter for offsets. Moreover, $\Delta P = P_1 - P_2$ denotes the differential pressure, may be considered a fourth state, and can be measured using the absolute pressure sensor [19]. It has been established that the fault conditions affect two types of parameters of the nonlinear model (34): the friction coefficients a_1, a_2, and a_3, and the leakage coefficient L. In order to model the EHA dynamics accurately, parameter values should be modified for each situation. Table 2 presents numerical values of the friction coefficients for different simulated fault conditions. These values are obtained by experimentation, as presented in [19]. Furthermore, Table 3 shows numerical values of the leakage coefficients and flow rate offsets for fault conditions.

Two case studies were considered. In the first case, the EHA model of (32) through (34) was linearized and was used for estimation under normal and uncertain conditions. In this case, the position x_1 was the only measurable state $\mathbf{H} = [\,1 \quad 0 \quad 0\,]$, whereas its velocity and acceleration were considered as hidden states. Hence, in this case $m < n$, the corrective gain of (28) should be applied. Note that artificial measurements need to be produced for the velocity and acceleration. They are respectively obtained by calculating the first and the second time-difference of the measured signal (which introduces noise). The produced velocity and acceleration data are used as artificial measurements, whereas they cannot directly be measured. In this context, since $m = n$, it allows for applying the gain (9) for state estimation using the nonlinear EHA model.

In the second case, the EHA's nonlinear model was directly used for estimation without any linearization or approximation. It was assumed that the position, velocity, and acceleration were measured, and hence $\mathbf{H} = \mathbf{eye}(3)$.

The test scenario is the same for each case and includes the normal EHA, the EHA with friction, and the EHA with internal leakage. The test is designed and conducted for 20 s. The EHA operates normally for the first 4 s, followed by friction for the next 8 s, and ends with leakage for the last 8 s. The EHA normal model is used by all of the filters (KF, SVSF, and NSO) for state estimation in order to provide consistent results and comparisons. The three state variables are initialized as zero. The input to the EHA is the motor angular velocity that is applied by a square wave signal oscillating between -100 and $+100$ rad/sec. Fig. 4 presents profiles of the input angular velocity and the output position measured by the optical encoder. The state estimate and state error covariance matrix are initialized as follows:

$$\hat{\mathbf{x}}_{0|0} = \begin{bmatrix} 0 & 0 & 0 \end{bmatrix}, \quad \mathbf{P}_{0|0} = 10 \times \mathbf{eye}(3). \tag{36}$$

For the standard SVSF strategy, the smoothing boundary layer width and the convergence rate are respectively defined as $\gamma = 0.5$ and $\psi = [\,10^{-10} \quad 10^{-8} \quad 10^{-4}\,]^T$. The convergence rate coefficient for the NSO filter is set to $\gamma = 0.5$. The following indicators are used to compare the state estimation methods: the root mean square (RMS) and the standard deviation (STD) of the state estimation error $\mathbf{e}_{x,}$. Note that a second-order Butterworth filter was applied to the velocity and acceleration signals in order to minimize

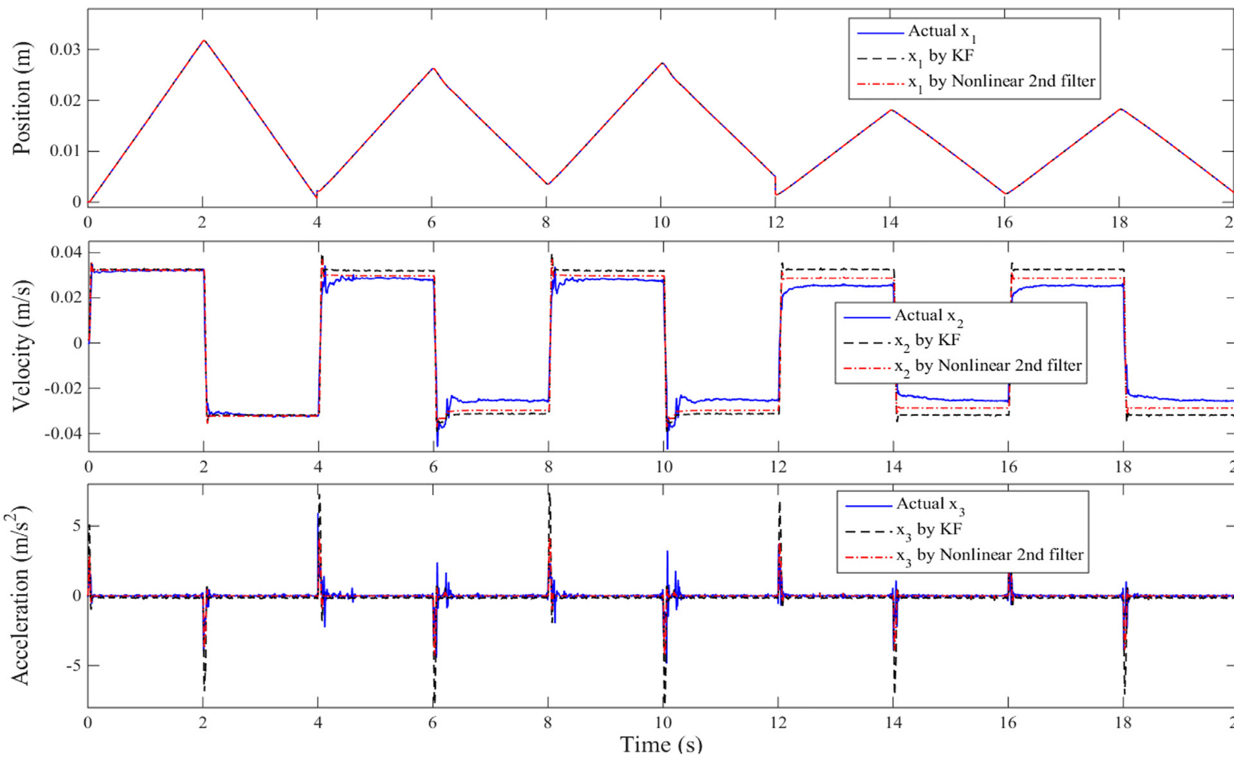

Fig. 5. Actual and estimated values obtained for the linear EHA model.

Table 4
Root mean square error.

State	Kalman filter	SVSF	NSO filter
Position (m)	7.82×10^{-7}	6.88×10^{-7}	3.39×10^{-7}
Velocity (m/s)	8.78×10^{-3}	7.63×10^{-3}	3.27×10^{-3}
Acceleration (m/s^2)	0.85	0.71	0.43

Table 5
Standard deviation.

State	Kalman filter	SVSF	NSO filter
Position (m)	7.41×10^{-7}	6.39×10^{-7}	3.17×10^{-7}
Velocity (m/s)	8.96×10^{-3}	7.72×10^{-3}	3.16×10^{-3}
Acceleration (m/s^2)	0.81	0.74	0.41

the amplification of noise (from the derivative of the measured position).

5.1. Case 1: linear EHA with position measurement only ($\mathrm{m} = \mathrm{n}$)

The nonlinear model of the EHA, described by (36) through (38), needs to be linearized in the first case study. The linearization is performed by calculating partial derivatives of the nonlinear model at its equilibrium point: $\mathbf{x}(0) = [\begin{matrix} 0 & 0 & 0 \end{matrix}]^T$. The linearized model of the EHA setup is described by:

$$\mathbf{x}_{k+1} = \mathbf{A}\mathbf{x}_k + \mathbf{B}\mathbf{u}_k, \tag{37}$$

where

$$\mathbf{A} = \begin{bmatrix} 1 & T & 0 \\ 0 & 1 & T \\ 0 & -60.303 & 0.708 \end{bmatrix}, \quad \mathbf{B} = \begin{bmatrix} 0 \\ 0 \\ 39497 \end{bmatrix}. \tag{38}$$

The system noise covariance **Q** and the measurement noise covariance **R** for the KF are defined as per the following:

$$\mathbf{Q} = \begin{bmatrix} 10^6 & 0 & 0 \\ 0 & 10^2 & 0 \\ 0 & 0 & 10^3 \end{bmatrix}, \quad \mathbf{R} = 10^{-10}. \tag{39}$$

Note that in this case study, since $m < n$, the Luenberger observer is used in conjunction with the filter gain to estimate actuator velocity and acceleration. In this context, the NSO filter with the corrective gain (28) applies for state estimation. Tables 4 and 5 respectively list the RMS and STD values of the estimation error. Fig. 5 shows the actual and estimated state trajectories for the EHA's linearized model. Fig. 6 presents profiles of the estimation error obtained by the KF and the NSO filter.

5.2. Case 2: nonlinear EHA with full measurements ($\mathrm{m} = \mathrm{n}$)

In this case, the nonlinear EHA model described by Eqs. (32) through (34) is utilized by the EKF, SVSF, and NSO strategies. It is assumed that all states are measurable, whereas measurements of the velocity and acceleration are respectively obtained by taking the first and second time-derivatives of the position measurement signal. The system noise covariance **Q** and the measurement noise covariance **R** for the EKF are defined as follows:

$$\mathbf{Q} = \begin{bmatrix} 10^6 & 0 & 0 \\ 0 & 10^2 & 0 \\ 0 & 0 & 10^3 \end{bmatrix}, \quad \mathbf{R} = \begin{bmatrix} 10^{-10} & 0 & 0 \\ 0 & 10^{-7} & 0 \\ 0 & 0 & 10^{-5} \end{bmatrix}. \tag{40}$$

In order to use the NSO filter, the corrective gain (9) applies, while the measurement matrix is equal to $\mathbf{H} = \mathbf{eye}(3)$. Table 6 and Table 7 respectively present the RMS and STD values of the estimation error obtained by estimators for the second case study. The EHA follows the same operating conditions as per the first case. The actual and the estimated states for the second case study are shown in Fig. 7. The state estimation error obtained by the EKF and the NSO filter are shown in Fig. 8. The measurement error

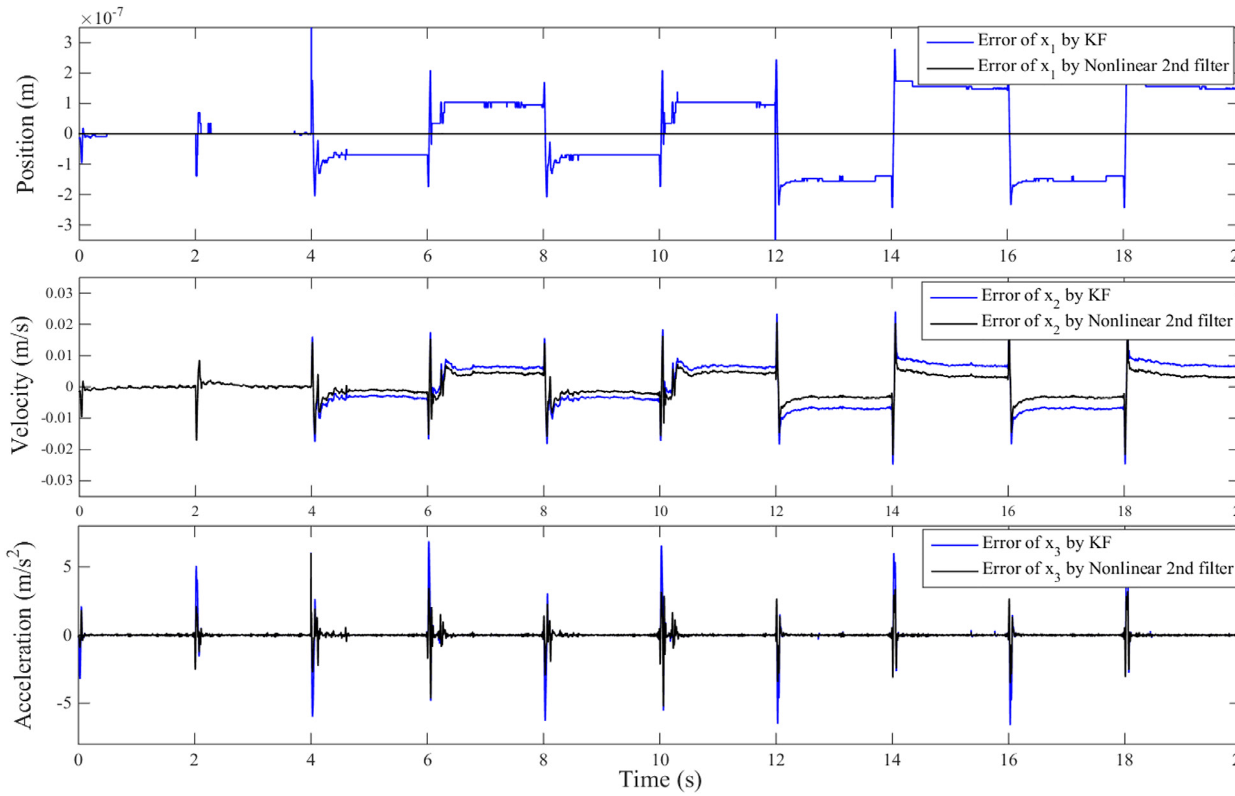

Fig. 6. Profiles of the estimation error for the linear EHA model.

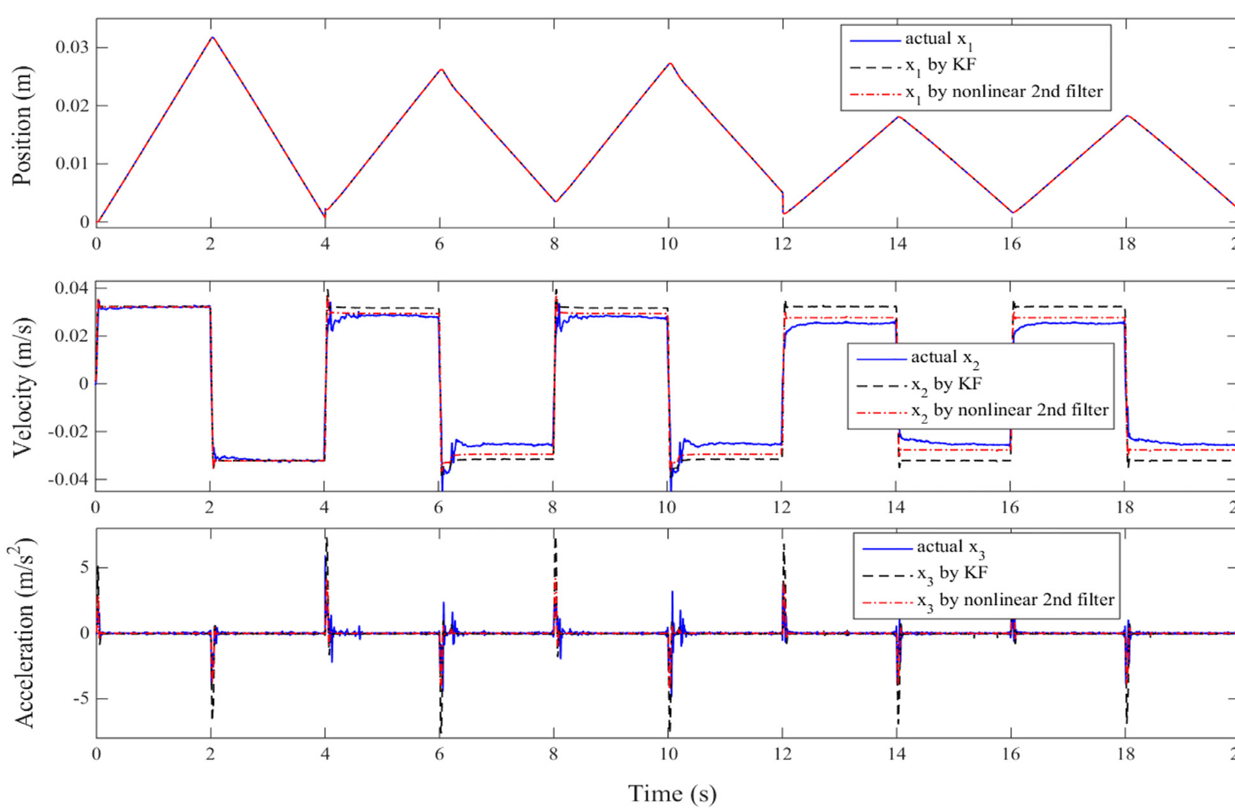

Fig. 7. Actual and estimated states with the nonlinear EHA model (KF refers to EKF).

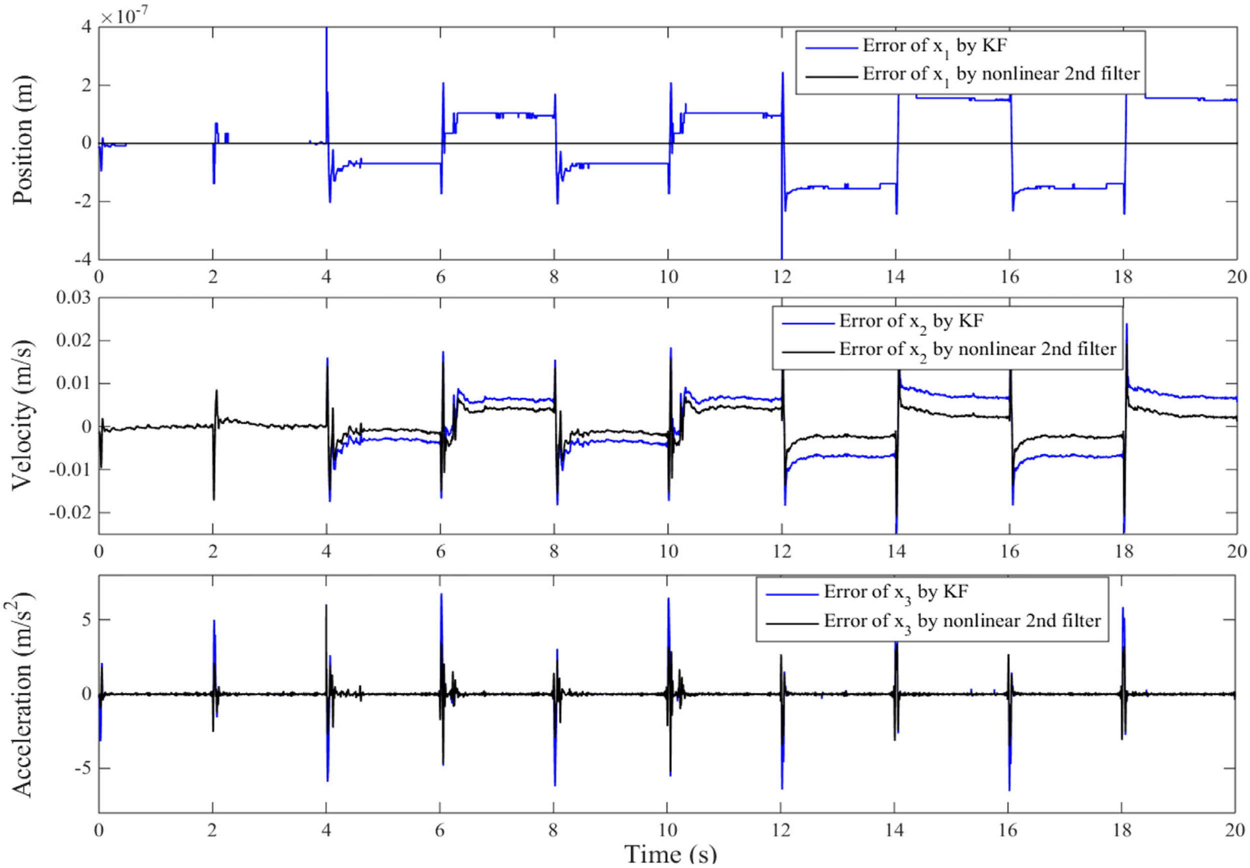

Fig. 8. Profiles of the estimation error with the nonlinear EHA model (KF refers to EKF).

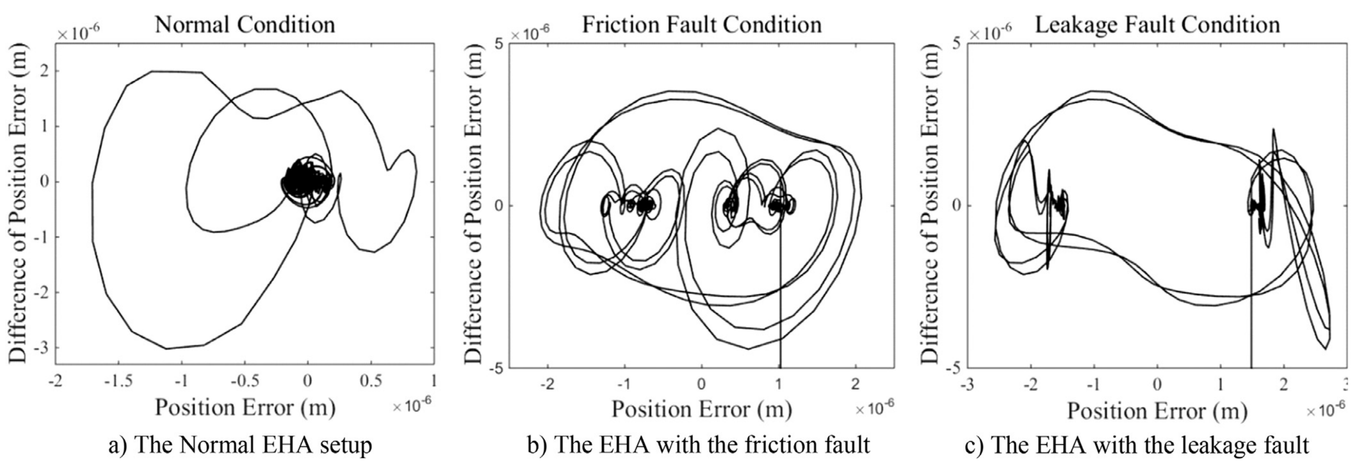

Fig. 9. Phase portraits of the measurement error and its difference obtained by the NSO filter.

Table 6
Root mean square error.

State	EKF	SVSF	NSO filter
Position (m)	7.24×10^{-7}	6.16×10^{-7}	3.15×10^{-7}
Velocity (m/s)	8.27×10^{-3}	7.11×10^{-3}	3.28×10^{-3}
Acceleration (m/s^2)	0.79	0.64	0.39

Table 7
Standard deviation.

State	EKF	SVSF	NSO filter
Position (m)	7.53×10^{-7}	6.28×10^{-7}	3.12×10^{-7}
Velocity (m/s)	8.58×10^{-3}	7.34×10^{-3}	3.22×10^{-3}
Acceleration (m/s^2)	0.81	0.69	0.35

obtained by the NSO filter is shown as a phase portrait in Fig. 9 for each condition.

5.3. Comparison and discussion

As illustrated in Tables 4 through 7, the proposed NSO filter provided the most accurate state estimates as per the smallest

RMS value, followed by the SVSF, and EKF (or KF) method. During the presence of faults, the filters do not model the EHA dynamics correctly, and as such, the KF fails to provide a robust estimate. This was expected since one of the main KF assumptions is that the modeled system is known. However, it is important to mention that under normal conditions the KF or EKF yields excellent tracking performance. Since the NSO filter preserves stability versus bounded uncertainties, it reduces the measurement error over time until reaching a subspace restricted by ε_e and $\varepsilon_{\Delta e}$. Thereafter, the state estimation error remains norm-bounded. Figs. 5 through 8 further illustrate the estimated state trajectories. Since the actuator position is directly measured, its trajectory is closely followed by state estimation trajectories even under faulty operating conditions. Moreover, it is presumed from the estimation results that the NSO filter is also more accurate than the SVSF. The NSO filter gain applies second-order constraints on the measurement error that does not require the saturation condition in which the discontinuous corrective action of the gain is approximated; thereby increasing the accuracy when compared with the SVSF.

Experimentations demonstrate that the NSO filter generates state estimates with the smallest STD, followed next by the SVSF and the EKF. The smoothness characteristic is specifically observed for the estimated acceleration trajectory. This verifies that the NSO filter provides smoother state estimates in comparison to other estimation methods due to the corrective gain of the NSO strategy defined by the second-order formulation. Moreover, Fig. 9 illustrates the phase portrait of the measurement error produced by the NSO filter for the second case study. As shown, the measurement error decreases over time until the estimates reach a region close to the true trajectory also known as the subspace (which is a function of ε_e and $\varepsilon_{\Delta e}$). The width of this subspace is based on the modeling uncertainties, measurement noise, discretization error, and even the number and magnitude of external disturbances. It is typically defined a designer value. However, it is observed that the measurement error remains bounded, even though this bound is larger for the faulty operating conditions.

6. Conclusion

A new estimation strategy referred to as the nonlinear second-order (NSO) filter was introduced and implemented in this paper. The NSO filter was derived based on variable structure control theory, and was formulated as predictor-corrector strategy that uses a corrective gain to recursively decrease the measurement error. The corrective gain of the NSO filter updates state estimates using measurement errors from the two previous time steps, which consequently provides the filter with more information for estimation. This gain formulation not only results in smoother state estimates, but also improves the estimation performance in terms of state estimation accuracy as well as robustness and stability to uncertainties. The NSO filter was implemented an experimental setup, and was compared with the popular KF, EKF, and SVSF strategies. Experimental results indicate that the proposed NSO strategy yields improved state estimates in terms of estimation error with the smallest RMS and STD values. In addition to robustness and smoothness advantages, the NSO filter offers application to nonlinear systems without any need for linearization or approximation. Since a higher-order version of the SVSF was derived, it was expected to yield a more accurate solution to the estimation problem in terms of state error. However, the higher-order accuracy comes at a trade-off with computational complexity and time. Future work will look at comparing the proposed strategy with other popular robust estimation strategies.

Appendix

The EHA consists of a number of different components, including: linear actuator (8), variable-speed electric motor (13), gear pump (10), pressure relief valve (7), accumulator (2), and safety circuits (Fig. A). The EHA setup also includes circuits that enable the physical simulation of leakage and friction faults. There are two pistons: piston (3) at the top and piston (4) at the bottom. The EHA uses pumping action (10) to create pressure and move piston *A* (3) and piston *B* (4). The servomotor controls the gear pump (10) and forces hydraulic oil into the cylinder (8). The gear pump (10) changes the linear actuator position (and speed) by controlling the flow rate and direction of hydraulic oil. An accumulator (12) is primarily used to avoid cavitation, and collects excess oil (10). The pressure relief valve (7) limits the maximum system pressure to 500 psi in this case study.

The hydraulic circuit contains two main parts. The first is a low-pressure circuit that filters the oil and ensures a minimum

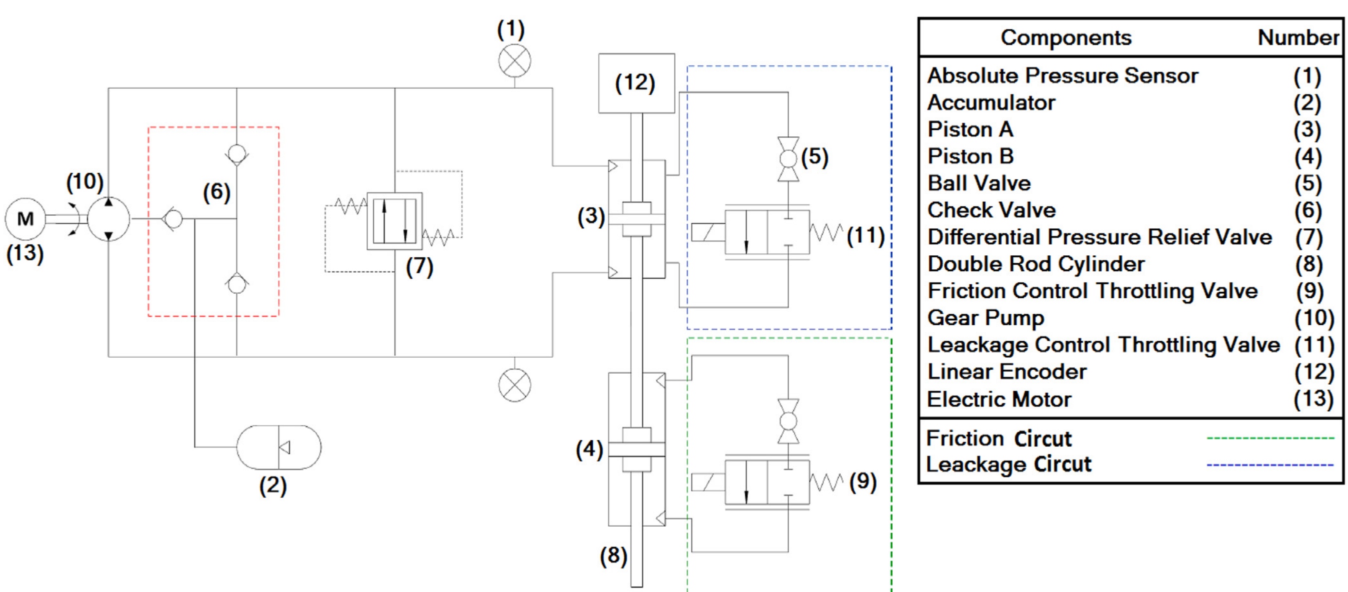

Fig. A. The EHA hydraulic circuit diagram (modified from [19]).

pressure of 40 psi by using an accumulator (2) as well as filters and check valves (6). The second is an outer high-pressure circuit that controls the linear actuator. The input to the EHA is the voltage to the electric motor (13), which controls the speed and direction of the pump (10). An optical linear encoder with a state resolution of 1 nm (12) is attached to piston *A*. Two main types of fault conditions were physically generated: internal leakage and friction. To implement a friction fault in the system, piston *A* was used as the driver while piston *B* was the load. To simulate internal leakage faults across the circuit, throttling valves for piston *A* and *B* were used in conjunction to create cross-port leakage. Based on this fault condition, the cylinder (8) response was affected.

References

[1] R.E. Kalman, A new approach to linear filtering and prediction problems, ASME J. Basic Eng. 82 (1960) 35–45.
[2] Y. Bar-Shalom, X. Rong Li, T. Kirubarajan, Estimation With Applications to Tracking and Navigation, John Wiley & Sons Inc, 2001.
[3] B. Ristic, B.S. Arulampalam, N. Gordon, Beyond the Kalman Filter: Particle Filters For Tracking Applications, Artech House, Boston, 2004.
[4] I. Arasaratnam, S. Haykin, Cubature Kalman filters, IEEE Trans. Autom. Control 54 (6) (2009) 1254–1269.
[5] M.S. Arulampalam, S. Maskell, N. Gordon, T. Clapp, A tutorial on particle filters for online nonlinear/non-Gaussian Bayesian tracking, IEEE Trans. Signal Process. 59 (2) (2002) 174–188.
[6] A. Doucet, N. Gordon, V. Krishnamurthy, Particle filters for state estimation of jump Markov linear systems, IEEE Trans. Signal Process. 49 (3) (2001) 613–624.
[7] M. Milanese, R. Tempo, Optimal algorithms theory for robust estimation and prediction, IEEE Trans. Autom. Control 30 (8) (1985) 730–738.
[8] S. Zhuk, Minimax state estimation for linear discrete-time differential algebraic equations, Automatica 46 (11) (2010) 1785–1789.
[9] M. Zorzi, On the robustness of the Bayes and Wiener estimators under model uncertainty, Automatica 83 (9) (2017) 133–140.
[10] M. Zorzi, Robust Kalman filtering under model perturbations, IEEE Trans. Autom. Control 62 (6) (2017) 2902–2907.
[11] L. Xie, C. Soh, C.E. Souza, Robust Kalman filtering for uncertain discrete-time systems, IEEE Trans. Autom. Control 39 (6) (1994) 1310–1314.
[12] F. Wang, V. Balakrishnan, Robust Kalman filters for linear time-varying systems with stochastic parameter uncertainties, IEEE Trans. Signal Process. 50 (4) (2002) 803–813.
[13] G. Zames, Feedback and optimal sensitivity: model reference transformations, multiplicative seminorms and approximate inverse, IEEE Trans. Autom. Control 26 (2) (1981) 301–320.
[14] A.J. Krener, Kalman-Bucy and minimax filtering, IEEE Trans. Autom. Control 25 (2) (1980) 291–292.
[15] M.A. Gandhi, L. Mili, Robust Kalman filter based on a generalized maximum–likelihood-type estimator, IEEE Trans. Signal Process. 58 (5) (2010) 2509–2520.
[16] S. Habibi, R. Burton, The variable structure filter, ASME J. Dyn. Syst. Meas. Control 125 (3) (2003) 287–293.
[17] S. Habibi, Smooth variable structure filter, Proc. IEEE 95 (5) (2007) 1026–1059.
[18] S.A. Gadsden, S. Habibi, A new robust filtering strategy for linear systems, ASME J. Dyn. Syst. Meas. Control 135 (1) (2013) 014503.
[19] S.A. Gadsden, Y. Song, S. Habibi, Novel model-based estimators for the purpose of fault detection and diagnosis, IEEE/ASME Trans. Mechatron. 18 (4) (2013) 1237–1249.
[20] S.A. Gadsden, S.R. Habibi, Model-based fault detection of a battery system in a hybrid electric vehicle, J. Energy Power Eng 7 (7) (2013) 1344–1351.
[21] S.A. Gadsden, A.S. Lee, Advances of the smooth variable structure filter: square-root and two-pass formulations, J. Appl. Remote Sens. 11 (1) (2017) 1–19.
[22] S.A. Gadsden, M. Al-Shabi, I. Arasaratnam, S.R. Habibi, Combined cubature Kalman and smooth variable structure filtering: a robust estimation strategy, Signal Process. 96 (B) (2014) 290–299.
[23] S.A. Gadsden, A.S. Lee, Advances of the smooth variable structure filter: square-root and two-pass formulations, J. Appl. Remote Sens. 11 (1) (2017).
[24] A. Zanj, H.H. Afshari, Dynamic analysis of a complex pneumatic valve using pseudo-bondgraph simulation technique, ASME J. Dyn. Syst. Meas. Control 135 (3) (2013).
[25] H.H. Afshari, A. Zanj, A.B. Novinzadeh, Dynamic analysis of a nonlinear pressure regulator using bondgraph simulation technique, J. Simul. Model. Pract. Theory 18 (2010) 240–252.
[26] H.H. Afshari, D. Al-Ani, S. Habibi, Robustness analysis of some state estimation methods with an explicit consideration of modeling uncertainties, in: Proceedings of the 28th IEEE Canadian Conference on Electrical and Computer Engineering, Halifax, NS, Canada, 2015.
[27] H.H. Afshari, S.A. Gadsden, S. Habibi, Condition monitoring of an electro-hydrostatic actuator using the dynamic 2nd-order smooth variable structure filter, in: Proceedings of the ASME International Design Engineering Technical Conferences & Computers and Information, Boston, Massachusetts, USA, 2015.
[28] H.H. Afshari, S.A. Gadsen, S. Habibi, Robust fault diagnosis of an electro-hydrostatic actuator using the novel optimal second-order SVSF and IMM strategies, Int. J. Fluid Power 15 (3) (2014) 181–196.
[29] H.H. Afshari, D. Al-Ani, S. Habibi, State estiamtion of a faulty actuator using the second-order smooth variable structure filter, in: Proceedings of the IEEE 28th Canadian Conference on Electrical and Computer Engineering, Halifax, Canada, 2015, pp. 919–924.
[30] M. Attari, H.H. Afshari, S. Habibi, Maneuvering car tracking using the interacting multiple model and the dynamic 2nd-order SVSF method, in: Proceedings of the ASME International Design Engineering Technical Conferences and Computers and Information in Engineering Conference, Boston, Massachusetts, USA, 2015.
[31] H.H. Afshari, D. Al-Ani, S. Habibi, A new adaptive control scheme based on the interacting multiple model (IMM) estimation, J. Mech. Sci. Technol. 30 (6) (2016) 2759–2767.
[32] H.H. Afshari, S.A. Gadsden, S.H. Habibi, Gaussian filters for parameter and state estimation: a general review of theory and recent trends, Signal Process. 135 (2017) 218–238.
[33] H.H. Afshari, M. Attari, R. Ahmed, M. Farag, S. Habibi, Modeling, parameterization, and state of charge estimation of Li-ion cells using a circuit model, in: Proceedings of the ITEC/IEEE Transportation Electrification Conference and Expo, Dearborn, Michigan, USA, 2016.
[34] S.A. Gadsden, Smooth Variable Structure Filtering: Theory and Applications, McMaster University, Hamilton, Ontario, 2011.